ACS APPLIED MATERIALS & INTERFACES

Research Article

www.acsami.org

Preparation and Ni-Doping Effect of Nanosized Truncated Octahedral $LiCoMnO_4$ As Cathode Materials for 5 V Li-Ion Batteries

Meng Hu, Yuan Tian, Liwei Su, Jinping Wei, and Zhen Zhou*

Tianjin Key Laboratory of Metal and Molecule Based Material Chemistry, Key Laboratory of Advanced Energy Materials Chemistry (Ministry of Education), Institute of New Energy Material Chemistry, Synergetic Innovation Center of Chemical Science and Engineering (Tianjin), Nankai University, Tianjin 300071, People's Republic of China

Supporting Information

ABSTRACT: $LiCoMnO_4$ with nanosized truncated octahedral structure was prepared via a modified sol–gel route. The single-crystalline subunits grew completely without serious agglomeration. The growth mechanism was discussed in detail. The sample was tested as cathode materials for 5 V Li-ion batteries. Ni doping was also investigated to decrease the content of Mn^{3+} ions and the Mn dissolution, and then the decomposition of electrolyte was inhibited on the cathode surface. $LiCo_{0.9}Ni_{0.1}MnO_4$ exhibited enhanced cyclic stability compared with the pristine $LiCoMnO_4$.

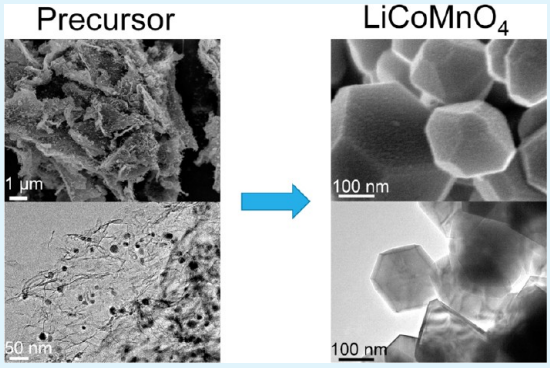

KEYWORDS: *$LiCoMnO_4$, lithium-ion batteries, cathodes, high voltage, doping*

INTRODUCTION

Lithium-ion batteries have been widely used as high-efficiency energy storage devices. However, the energy density still needs to be improved to fulfill the ever increasing demands.[1] The spinel $LiMn_2O_4$ has been extensively studied because of good electrochemical performance, low cost, and high safety.[2] However, the application of $LiMn_2O_4$ is limited because of the low energy density, which is restricted by its small theoretical capacity and moderate discharge potential. Increasing the discharge potential is the only strategy to improve the energy density of the spinel-type cathode materials because of the inflexibility of their theoretical capacity.[3] $LiNi_{0.5}Mn_{1.5}O_4$ is a typical example and exhibits a flat discharge plateau around 4.7 V vs. Li/Li^+. Compared with $LiNi_{0.5}Mn_{1.5}O_4$, $LiCoMnO_4$ with the Co^{2+}/Co^{3+} redox couple demonstrates even higher discharge potential at ~5.0 V vs. Li/Li^+,[4,5] and displays higher energy density accordingly.

$LiCoMnO_4$ exhibits a spinel structure with the space group of $Fd\bar{3}m$. The valence of the Mn ions is promoted to +4. Because of the oxygen loss under high preparation temperatures, Mn^{3+} ions reduced from Mn^{4+} ions are observed in the non-stoichiometric $LiCoMnO_{4-\delta}$.[6−9] Small amount of Mn^{3+} ions could improve the electronic conductivity and benefit the rate performance of the materials.[10] However, more Mn^{3+} ions would cause the irreversible structural transition from spinel to tetragonal structure because of the Jahn–Teller distortion and the dissolution of Mn ions in the electrolytes,[11,12] which degrade the cyclic and elevated-temperature performance. Therefore, the content of Mn^{3+} ions in $LiCoMnO_4$ should be well controlled.

On the other hand, the morphology control of the cathode materials is always a challenge because of the phase formation process under high temperatures for a long time. $LiCoMnO_4$ cathode materials were prepared through direct solid state reactions or sol–gel methods according to the previous reports.[13,14] These methods result in serious agglomeration and large particles, which hinder the Li^+ diffusion. In addition, it has been reported that the surface crystallographic planes affect the electrochemical performances of the materials.[15−17] The formation of solid electrolyte interfacial (SEI) films and the Mn dissolution ratio are diverse on different crystal planes.[18,19] Therefore, preparing $LiCoMnO_4$ with particular morphologies and crystal planes is highly desired.

For cathode materials in 5 V Li-ion batteries, the surface side reaction with the electrolytes is another key problem that influences the cyclic stability. Compared with $LiCoMnO_4$, $LiNi_{0.5}Mn_{1.5}O_4$ exhibits excellent stability in the organic electrolytes even at 5.2 V vs. Li/Li^+,[20] indicating that the Ni ions in spinels provide less catalytic activity to decompose the electrolyte than Co ions. Substituting Ni ions for part of Co ions could decrease the surface content of Co ions and inhibit the decomposition of the electrolyte accordingly. The low-valence Ni^{2+} would promote more Mn^{3+} to Mn^{4+}, and decrease

Received: September 27, 2013
Accepted: October 29, 2013
Published: October 29, 2013

the Mn dissolution.[21,22] In addition, the Ni-doping ions are also electrochemically active, which will not decrease the discharge capacity.

In this work, we proposed a modified sol−gel method to prepare nanosized truncated octahedral $LiCoMnO_4$ cathode materials, and the growth mechanism was also discussed. Ni doping was then investigated to improve the cyclic stability of the $LiCoMnO_4$ cathode material.

EXPERIMENTAL SECTION

Material Preparation. One millimole of $Co(NO_3)_2{\cdot}6H_2O$, 1 mmol of $MnCl_2{\cdot}4H_2O$, 1 mmol of $LiNO_3$, 1 g of citric acid, and 10 g of urea were dissolved in 200 mL of water/ethanol mixed solvents with magnetic agitation. The solution was stirred at 75 °C to remove the excess water, and then the resultant gel was dried at 100 °C in air. The precursor was obtained by calcining the gel at 350 °C for 4 h and then at 650 °C for 10 h in flowing argon. The precursor was ground and further calcined at 500 °C for 6 h and then at 800 °C in air. To investigate the growth mechanism of the $LiCoMnO_4$ particles, we calcined the precursors at 800 °C for different times. The Ni-doped $LiCo_{0.9}Ni_{0.1}MnO_4$ sample was obtained by adding stoichiometric amounst of $Ni(NO_3)_2{\cdot}6H_2O$ to the starting materials.

Material Characterization. The crystal structures of the samples were determined by a D/MAX III X-ray diffraction (XRD) diffractometer with Cu Kα radiation. The morphology was observed by a JEOL-JSM7500 field emission scanning electron microscope (FESEM). The composition of the samples was confirmed by energy dispersive X-ray spectroscopy (EDS) attached to the FESEM instrument. A FEI Tecnai G^2F-20 field emission transmission electron microscope (TEM) was used to investigate the microstructures of the samples. Thermogravimetry and differential thermal analysis (TG-DTA, Rigaku PTC-10A) were taken to determine the appropriate preparation temperature. Surface element analysis was performed by X-ray photoelectron spectroscopy (XPS, Axis Ultra DLD, Kratos Analytical Ltd.), and the sputtering was performed with an argon ion beam gun for 5 min.

Electrochemical Tests. The cathodes were composed of active material, acetylene black, and polyvinylidene fluoride (PVDF) binder with a weight ratio of 80:10:10, which were mixed homogeneously and pasted on aluminum foil. The electrolyte was 1 M $LiPF_6$ dissolved in a mixture of ethylene carbonate (EC), ethyl methyl carbonate (EMC) and dimethyl carbonate (DMC) (1:1:1 by volume). CR2025-type coin cells were assembled with lithium metal as anodes in an argon-filled glove box. Galvanostatic charge/discharge tests were performed on a Land CT2001 battery tester between 3.0 and 5.3 V at room temperature (25 °C). Cyclic voltammetry (CV) was measured on a Zahner-Elektrik IM6e electrochemical workstation with a scan rate of 0.1 mV s^{-1} between 3.0 and 5.4 V at room temperature.

RESULTS AND DISCUSSION

The XRD patterns of the precursor and the $LiCoMnO_4$ samples are shown in Figure 1a. The diffraction peaks of the precursor could be indexed as MnO, Co, and graphitized carbon. The Co-containing compounds are reduced to metal because of the highly reductive atmosphere, whereas the Mn salts are more difficult to be reduced. Our earlier report demonstrated that the Ni salts were also reduced to metals.[23] The diffraction peaks of the product are indexed to spinel structure with the space group of $Fd\bar{3}m$ and are consistent with the previous reports.[8,24] The $LiCo_{0.9}Ni_{0.1}MnO_4$ sample exhibits similar diffraction peaks except that the peaks integrally shift to smaller angles due to the larger radius of Ni^{2+} compared with Co^{3+} and Mn^{4+} (Figure 1b). The calculated lattice parameters, a, of the $LiCoMnO_4$ and $LiCo_{0.9}Ni_{0.1}MnO_4$ samples are 0.8068 and 0.8095 nm, respectively.

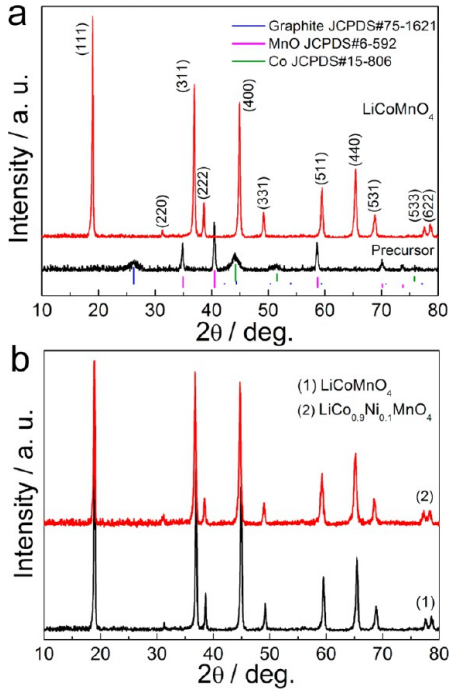

Figure 1. XRD patterns of the precursor, the pristine, and Ni-doped $LiCoMnO_4$ samples.

The morphology of the precursor is shown in panels a and b in Figure 2. The precursor is stacked by carbon sheets with the thickness of ∼200 nm. The elemental mappings of the precursor based on Figure 2b are shown in Figure 2e−h, from which we can see that C, Co, Mn, and O elements are homogeneously distributed. Images c and d in Figure 2 show the TEM images. The MnO and Co particles are widely dispersed in the carbon sheets with the diameter of 10−20 nm. The massive urea promotes the dispersion of the citric acid and then the formation of the carbon sheets, which further avoid the agglomeration of the metal and metal oxide, allowing for the generation of extremely small particles.

To determine the preparation temperature of $LiCoMnO_4$, we took TG-DTA in air (see Figure S1 in the Supporting Information). A remarkable weight loss is observed at ∼350 °C with a sharp exothermic peak, which is mainly due to the oxidation of carbon. The oxidation of the metal Co also occurs during this process. Therefore, 500 °C is chosen as the pre-calcination temperature of the precursor to remove the carbon, and then the samples were calcinated at 800 °C for different times to investigate the growth mechanism and determine the appropriate calcination time. The morphology of the obtained samples is shown in Figure 3. After calcinated at 500 °C for 6 h, the sample is composed of small particles with the diameters of 20−50 nm, which only slightly agglomerate. When further calcinated at 800 °C for 3 h, the small particles agglomerated together and larger particles with the diameters of ∼200 nm emerged. The irregular particles started to crystallize when calcinated at 800 °C for 6 h. The resultant crystals did not grow completely yet, and the neighboring crystals did not exhibit entire crystal planes. After calcinated at 800 °C for 12 h, complete crystals generated with the truncated octahedral structure, which are uniform with smooth planes. After calcinated at 800 °C for 18 h, the edges of the crystals became indistinct and the surfaces trend to be rough, due to the serious oxygen loss accompanied with the transformation from spinel

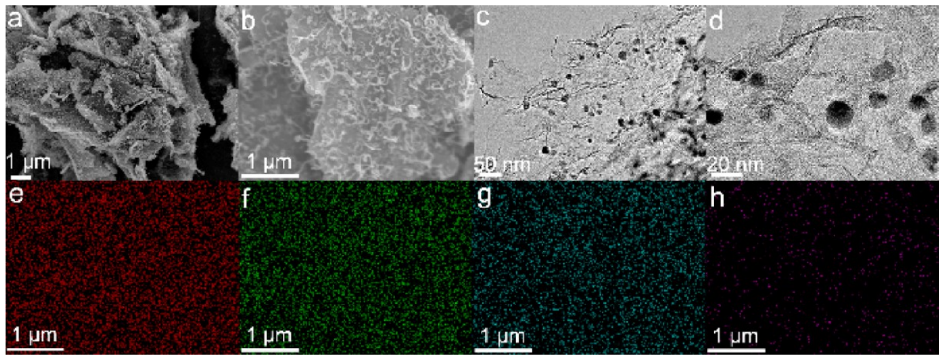

Figure 2. (a, b) SEM and (c, d) TEM images of the precursor; EDS mappings of (e) C, (f) Co, (g) Mn, and (h) O of the precursor.

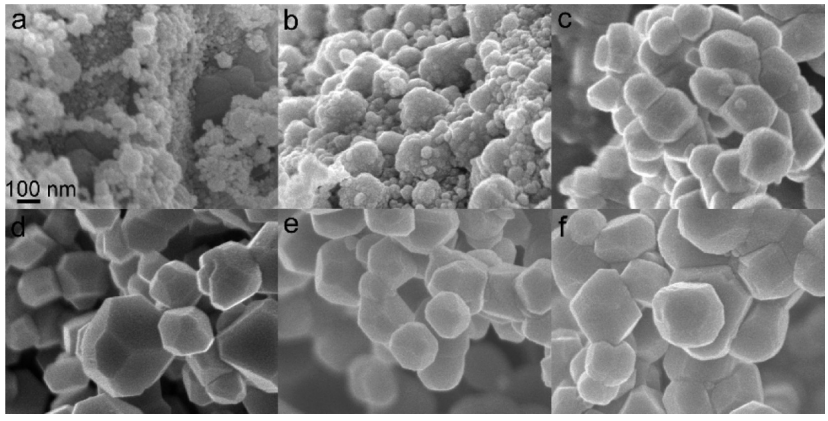

Figure 3. SEM images of the precursor calcinated at (a) 500 °C for 6 h followed by calcinated at 800 °C for (b) 3 , (c) 6, (d) 12, (e) 18, and (f) 24 h, respectively.

to rock salt. The phenomena were more obvious when calcinated at 800 °C for 24 h. The particles agglomerated conspicuously, and the morphology could not be maintained. Therefore, the $LiCoMnO_4$ sample calcinated for 12 h was chosen in the following studies. The microstructures of the $LiCoMnO_4$ sample calcinated at 800 °C for 12 h are shown in Figure 4, which displays regular truncated octahedral particles of ~200 nm in size. From the TEM image in Figure 4b, two kinds of crystal planes are clearly observed, which are squares and asymmetric hexagons. The high-resolution TEM (HRTEM) image and the fast Fourier transform (FFT) pattern (Figure 4c and inset) further reveal single crystalline character of the subunits, and determine the (111) crystal planes of the spinel phase. The EDS (Figure 4d) indicates that the Co/Mn ratio in the sample is close to 1:1. The Ni-doped sample also exhibits similar morphology (Figure 5), and the EDS confirms the composition of the sample.

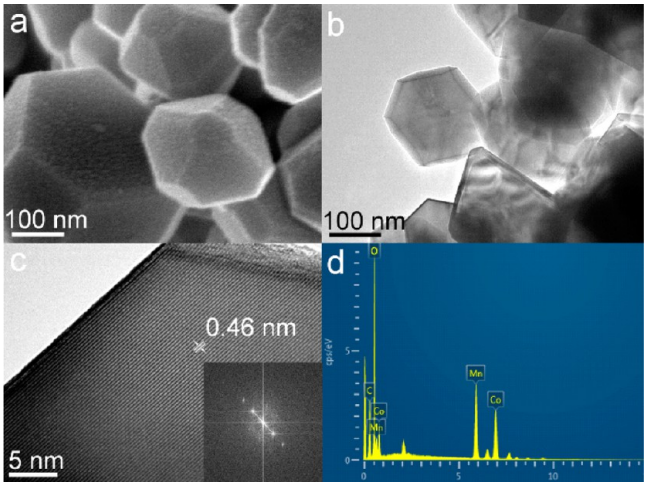

Figure 4. (a) SEM, (b) TEM, (c) HRTEM (the inset was the corresponding FFT pattern) images, and (d) EDS of the $LiCoMnO_4$ sample.

The $LiCoMnO_4$ material prepared by conventional sol–gel method in previous studies seriously agglomerated with the diameters of ~400 nm, and the particles were very irregular.[14] Herein, the metal ions chelated with citric acid are widely dispersed in massive urea, and then the metal and metal oxide nanoparticles are effectively distributed in carbon nanosheets without agglomeration in the calcination process under Ar. Carbon nanosheets with great quantity further inhibit the agglomeration of the metal oxide precursor under the phase formation process. The particles could grow to integrated single-crystalline subunits with the particular truncated octahedral structure and uniform particle size.

XPS was used to determine the surface and interior element contents of the $LiCoMnO_4$ and $LiCo_{0.9}Ni_{0.1}MnO_4$ samples (Table 1). It is striking to observe that the content of Co in the $LiCoMnO_4$ surface is obviously lower than that of Mn, indicating that part of Mn ions are +3 in valence. After sputtering for 5 min by argon ions, the Co/Mn mass ratio increases and approaches to the theoretical value, which illustrates that the Mn^{3+} ions mainly exist in the $LiCoMnO_4$ surface. For the $LiCo_{0.9}Ni_{0.1}MnO_4$ sample, the Co content in the surface further decreases because of the Ni doping. The

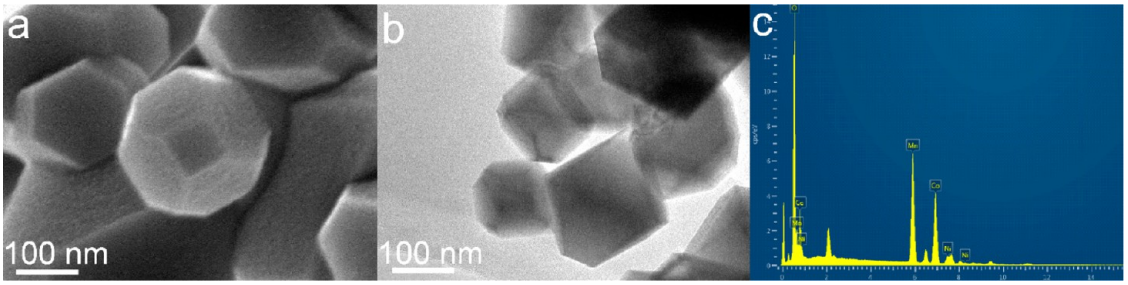

Figure 5. (a) SEM, (b) TEM, and (c) EDS of the $LiCo_{0.9}Ni_{0.1}MnO_4$ sample.

Table 1. Surface and Interior Contents of Co, Mn, and Ni in the Pristine and Ni-Doped $LiCoMnO_4$

	$LiCoMnO_4$		$LiCo_{0.9}Ni_{0.1}MnO_4$		
content	Co	Mn	Co	Mn	Ni
theoretical (wt %)	51.75	48.25	46.59	48.26	5.15
surface (wt %)[a]	45.91	54.09	42.29	48.29	9.42
interior (wt %)[a]	50.77	49.23	47.82	47.52	4.36

[a]Relative error <5%.

(Co+Ni)/Mn atomic ratio is 99.87%, suggesting that the content of Mn^{3+} ions largely decreases compared with the pristine $LiCoMnO_4$ sample. The Ni content in the surface is conspicuously higher than the theoretical value; Ni ions tend to be enriched in the surface. The enrichment of the doping ions in the surface is consistent with the previous report.[25] The Ni enrichment and Co deficiency, as well as the decrease of Mn^{3+} ions in the surface will benefit the performances of the $LiCoMnO_4$ cathode materials for 5 V Li-ion batteries.

The electrochemical performances of the pristine and Ni-doped $LiCoMnO_4$ samples were studied subsequently. The CV curves are shown in Figure 6a. For the pristine $LiCoMnO_4$, there are two pairs of peaks around 5 V vs. Li/Li^+, which come from the two-step extraction/insertion of Li^+ ions.[26] After Ni doping, a new pair of peaks emerges around 4.7 V, which represents the oxidation/reduction of Ni ions. It is clearly observed that the Ni-doped $LiCo_{0.9}Ni_{0.1}MnO_4$ cathodes exhibit smaller difference between the anodic and the corresponding cathodic peaks, indicating better reversibility of the electrodes compared with the pristine $LiCoMnO_4$ electrodes. The peaks around 4 V are attributed to the Mn^{3+}/Mn^{4+} redox couple. After Ni doping, the integral area of the peaks is decreased because of the lower content of Mn^{3+} ions.

The initial galvanostatic charge/discharge curves are shown in Figure 6b, at a rate of 1 C (145 mA g^{-1}), and the charge/discharge curves at the 2nd and 50th cycles are shown in Figure S3 in the Supporting Information. The charge plateaus are consistent with the CV curves. After doping with Ni ions, the capacity from the plateau at 4 V is decreased obviously, indicating lower content of Mn^{3+} ions. The discharge plateaus of the Co ions and Ni ions are successive, and the discharge capacity around 4 V is also reduced. Both samples exhibit contiguous discharge capacities (102.7 and 103.9 mAh g^{-1}, respectively). The cells were also tested at different rates. When tested at higher rates (Figure 6c), $LiCo_{0.9}Ni_{0.1}MnO_4$ exhibits higher capacity retention (the rate of the capacity at high rate

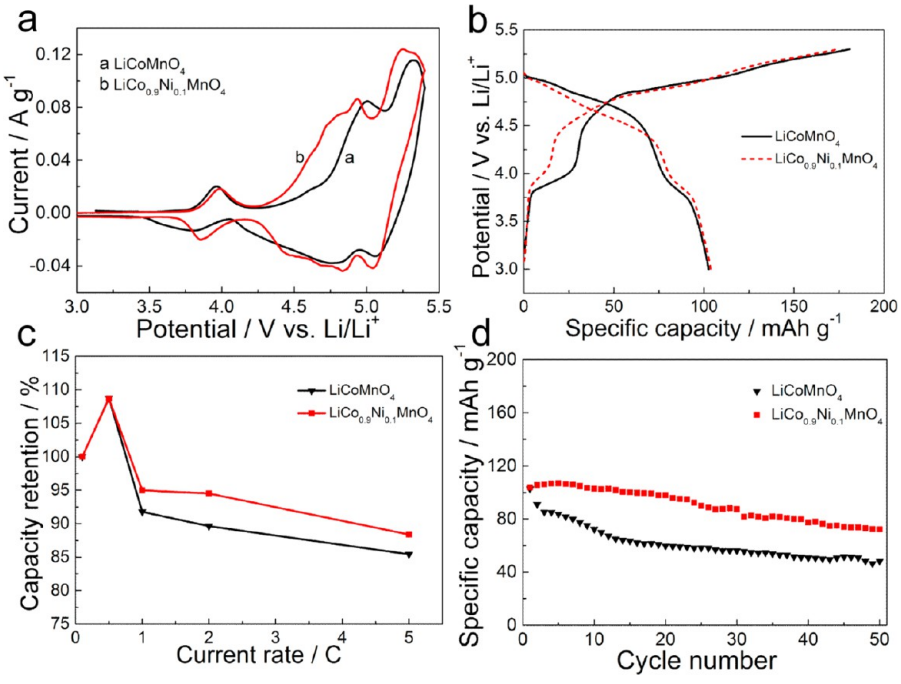

Figure 6. (a) CV curves, (b) initial galvanostatic charge/discharge curves at 1 C, (c) capacity retention at different rates, and (d) cyclic performance at 1 C of the $LiCoMnO_4$ and $LiCo_{0.9}Ni_{0.1}MnO_4$ samples.

vs. that at 0.1 *C*). It is anomalous that the capacities of both samples increase consistently with increasing the test rate from 0.1 to 0.5 *C*. Extremely large irreversible capacities can be observed at 0.1 *C* from the charge/discharge curves (see Figure S2 in the Supporting Information), indicating that the electrolyte was seriously decomposed at high potentials and thick SEI films would form accordingly, which would degrade the subsequent discharge performance at 0.1 *C*. Such phenomenon was not so significant at high rates (i.e., within short charge time). The abnormally higher capacity at a higher rate was also observed in other spinel cathodes.[10,27] Essentially, these confusing results originate from unstable electrolytes at high potentials, which should be optimized for high-voltage Li-ion batteries. Nevertheless, the $LiCo_{0.9}Ni_{0.1}MnO_4$ sample shows higher capacities at high rates than the pristine one.

The cyclic performance of $LiCoMnO_4$ and $LiCo_{0.9}Ni_{0.1}MnO_4$ is shown in Figure 6d, tested at 1 *C*. The $LiCo_{0.9}Ni_{0.1}MnO_4$ sample exhibits enhanced cyclic performance. The discharge capacity of the $LiCo_{0.9}Ni_{0.1}MnO_4$ sample is 72.2 mAh g^{-1} (69.5% of its initial capacity) after 50 cycles, whereas the pristine $LiCoMnO_4$ only retains 46.9% of its initial capacity. Also, the Coulombic efficiency of $LiCo_{0.9}Ni_{0.1}MnO_4$ is a little higher than that of pristine $LiCoMnO_4$ at 1 *C* (see Figure S4 in the Supporting Information). Compared with the previous reports,[4,14,24,28] the $LiCo_{0.9}Ni_{0.1}MnO_4$ sample exhibited better cyclic stability.

The cyclic stability of the $LiCoMnO_4$ cathode materials degrades because of the serious side reactions with the electrolyte, the Jahn–Teller distortion, and the dissolution of Mn ions in the electrolyte. The decomposition of the electrolyte on $LiCoMnO_4$ cathodes is more serious than on $LiNi_{0.5}Mn_{1.5}O_4$ cathodes, indicating that Co ions in spinels exhibit higher catalytic activity to decompose the electrolyte than Ni ions. Ni doping decreases the surface content of Co ions and then the decomposition of the electrolyte to some degree. In addition, the lower content of Mn^{3+} ions would also reduce the Jahn–Teller distortion and the dissolution of Mn ions in the electrolyte. Therefore, Ni doping enhances the cyclic stability of $LiCoMnO_4$ cathode material. To further improve the cyclic stability of the $LiCoMnO_4$ cathode materials, it is necessary to modify the surface of the materials and optimize the electrolytes.

CONCLUSION

In summary, $LiCoMnO_4$ with nanosized truncated octahedral structures was prepared through a modified sol-gel method, and tested as a cathode material for 5 V Li-ion batteries. The massive carbon nanosheets enabled the complete growth of single-crystalline particles without serious agglomeration. The effects of reaction time on the morphology of the particles were studied in detail. Ni doping was also investigated to control the content of the Mn^{3+} ions and decrease the decomposition of the electrolyte on the cathode surface. $LiCo_{0.9}Ni_{0.1}MnO_4$ exhibited better cyclic stability compared with the pristine $LiCoMnO_4$. The results would contribute to morphology control and performance improvement of $LiCoMnO_4$ cathode materials for 5 V Li-ion batteries.

ASSOCIATED CONTENT

Supporting Information

TG-DTA curves of the precursor, charge/discharge curves of $LiCoMnO_4$ and $LiCo_{0.9}Ni_{0.1}MnO_4$ at different rates and for various cycles, and Coulombic efficiency of $LiCoMnO_4$ and $LiCo_{0.9}Ni_{0.1}MnO_4$ cycled at 1 *C*. This material is available free of charge via the Internet at http://pubs.acs.org.

AUTHOR INFORMATION

Corresponding Author

*E-mail: zhouzhen@nankai.edu.cn.

Notes

The authors declare no competing financial interest.

ACKNOWLEDGMENTS

This work was supported by KST Battery Material Company in China.

REFERENCES

(1) Goodenough, J. B.; Kim, Y. *Chem. Mater.* **2010**, *22*, 587–603.
(2) Xu, B.; Qian, D.; Wang, Z.; Meng, Y. S. *Mater. Sci. Eng. R* **2012**, *73*, 51–65.
(3) Hu, M.; Pang, X.; Zhou, Z. *J. Power Sources* **2013**, *237*, 229–242.
(4) Kawai, H.; Nagata, M.; Tukamoto, H.; West, A. R. *Electrochem. Solid-State Lett.* **1998**, *1*, 212–214.
(5) Hu, M.; Tian, Y.; Wei, J.; Wang, D.; Zhou, Z. *J. Power Sources*, **2014**, *247*, 794–798.
(6) Stoyanova, R. K.; Zhecheva, E. N.; Gorova, M. Y. *J. Mater. Chem.* **2000**, *10*, 1377–1381.
(7) Reeves, N.; Kirk, C. A.; West, A. R. *J. Mater. Chem.* **2001**, *11*, 249–250.
(8) Mandal, S.; Rojas, R. M.; Amarilla, J. M.; Calle, P.; Kosova, N. V.; Anufrienko, V. F.; Rojo, J. M. *Chem. Mater.* **2002**, *14*, 1598–1605.
(9) Pasero, D.; de Souza, S.; Reeves, N.; West, A. R. *J. Mater. Chem.* **2005**, *15*, 4435–4440.
(10) Lazarraga, M. G.; Pascual, L.; Gadjov, H.; Kovacheva, D.; Petrov, K.; Amarilla, J. M.; Rojas, R. M.; Martin-Luengo, M. A.; Rojo, J. M. *J. Mater. Chem.* **2004**, *14*, 1640–1647.
(11) Song, J.; Shin, D. W.; Lu, Y.; Amos, C. D.; Manthiram, A.; Goodenough, J. B. *Chem. Mater.* **2012**, *24*, 3101–3109.
(12) Li, X.; Xu, Y. *J. Solid State Electrochem.* **2007**, *12*, 851–855.
(13) Kawai, H.; Nagata, M.; Kageyama, H.; Tukamoto, H.; West, A. R. *Electrochim. Acta* **1999**, *45*, 315–327.
(14) Huang, X.; Lin, M.; Tong, Q.; Li, X.; Ruan, Y.; Yang, Y. *J. Power Sources* **2012**, *202*, 352–356.
(15) Kim, J. S.; Kim, K.; Cho, W.; Shin, W. H.; Kanno, R.; Choi, J. W. *Nano Lett.* **2012**, *12*, 6358–6365.
(16) Chemelewski, K. R.; Shin, D. W.; Li, W.; Manthiram, A. *J. Mater. Chem. A* **2013**, *1*, 3347–3354.
(17) Chemelewski, K. R.; Lee, E.-S.; Li, W.; Manthiram, A. *Chem. Mater.* **2013**, *25*, 2890–2897.
(18) Hirayama, M.; Ido, H.; Kim, K.; Cho, W.; Tamura, K.; Mizuki, J. I.; Kanno, R. *J. Am. Chem. Soc.* **2010**, *132*, 15268–15276.
(19) Leung, K. *J. Phys. Chem. C* **2012**, *116*, 9852–9861.
(20) Xu, W.; Chen, X.; Ding, F.; Xiao, J.; Wang, D.; Pan, A.; Zheng, J.; Li, X. S.; Padmaperuma, A. B.; Zhang, J.-G. *J. Power Sources* **2012**, *213*, 304–316.
(21) Li, X.; Xu, Y. *Appl. Surf. Sci.* **2007**, *253*, 8592–8596.
(22) Li, X.; Xu, Y.; Wang, C. *J. Alloys Compd.* **2009**, *479*, 310–313.
(23) Su, L.; Zhou, Z.; Shen, P. *J. Phys. Chem. C* **2012**, *116*, 23974–23980.
(24) Alcántara, R.; Jaraba, M.; Lavela, P.; Tirado, J. L. *Chem. Mater.* **2003**, *15*, 1210–1216.
(25) Liu, J.; Manthiram, A. *J. Phys. Chem. C* **2009**, *113*, 15073–15079.
(26) Alcántara, R.; Jaraba, M.; Lavela, P.; Tirado, J. L. *J. Electrochem. Soc.* **2004**, *151*, A53–A58.
(27) Zhou, L.; Zhao, D.Y.; Lou, X.W. *Angew. Chem., Int. Ed.* **2012**, *51*, 239–241.
(28) Amarilla, J. M.; Rojas, R. M.; Pico, F.; Pascual, L.; Petrov, K.; Kovacheva, D.; Lazarraga, M. G.; Lejona, I.; Rojo, J. M. *J. Power Sources* **2007**, *174*, 1212–1217.